Journal of Solid State Chemistry 186 (2012) 9–16

Contents lists available at SciVerse ScienceDirect

Journal of Solid State Chemistry

journal homepage: www.elsevier.com/locate/jssc

Hydrogen atom distribution and hydrogen induced site depopulation for the $La_{2-x}Mg_xNi_7$–H system ☆

Matylda N. Guzik [a,b,*], Bjørn C. Hauback [b], Klaus Yvon [c]

[a] Laboratory of Crystallography, University of Geneva, 24 Quai Ernest Ansermet, CH-1211 Geneva, Switzerland
[b] Physics Department, Institute for Energy Technology, P.O. Box 40, NO-2027 Kjeller, Norway
[c] MANEP, Physics Department, University of Geneva, 24 Quai Ernest Ansermet, CH-1211 Geneva, Switzerland

ARTICLE INFO

Article history:
Received 20 September 2011
Received in revised form
14 November 2011
Accepted 15 November 2011
Available online 25 November 2011

Keywords:
Metal hydrides
Ni–MH batteries
A_2B_7-structure type
X-ray diffraction
Neutron diffraction

ABSTRACT

$La_{2-x}Mg_xNi_7$ and its hydrides/deuterides were investigated by high resolution synchrotron powder X-ray and neutron diffraction. Upon deuteration the single phase sample of the intermetallic compound with the refined composition $La_{1.63}Mg_{0.37}Ni_7$ (space group: $P6_3/mmc$) expands isotropically, in contrast to the Mg free phase. The hydrogen uptake, ~9 D/f.u., is higher than in $La_2Ni_7D_{6.5}$. The refined composition accounts for $La_{1.63}Mg_{0.37}Ni_7D_{8.8}$ (beta-phase). Rietveld refinements using the neutron and synchrotron diffraction data suggest that deuterium atoms occupy 5 different interstitial sites within both AB_2 and AB_5 slabs, either in an ordered or a disordered way. All determined D sites have an occupancy > 50% and the shortest D–D contact is 1.96(3) Å. It is supposed that a competition between the tendency to form directional bonds and repulsive D–D (H–H) interactions is the most important factor that influences the distribution of deuterium atoms in this structure.

A hitherto unknown second, alpha-phase with composition $La_{1.63}Mg_{0.37}Ni_7D_{0.56}$, crystallizing with the same hexagonal symmetry as $La_{1.63}Mg_{0.37}Ni_7D_{8.8}$, has been discovered. The unit cell parameters for this D-poor phase differ slightly from those of the intermetallic. Alpha-phase displays only one D site (*4f*, space group: $P6_3/mmc$) occupied > 50%, which is not populated in the D-rich beta-phase. This hydrogen/deuterium induced site depopulation can be explained by repulsive D–D (H–H) interactions that are likely to influence non-occupancy of certain interstices in metal lattice when absorbing hydrogen.

1. Introduction

For the last decade, the hydrides in La–Mg–Ni system have been a subject of numerous studies motivated by the discovery of superior electrochemical properties compared to Mg free compositions [1–10]. In particular, compounds with composite structure, e.g. AB_3, A_2B_7, A_5B_{19} with *A*—rare earth and *B*—transition element, so called superlattice compounds, attract attention due to their recent application in rechargeable Ni–MH batteries [1,3,9–22]. High hydrogen capacity, moderate hydrogen equilibrium pressure as well as light and less expensive elements makes them remarkable from an economical point of view. On the other hand, unknown structural properties raise the need for basic, crystallographic research. Recently, details about the structures of $Ce_2Ni_7H_{4/4.7}$ [23,24], $La_2Ni_7H_{6.5}$ [25], $La_2Ni_7H_x$ (x=6.4, 10.8) [10] and $La_4MgNi_{19}H(D)_x$ [13,15,16] have been published, but little is known about the (La, Mg)$_2$Ni$_7$–H system. The effect of Mg substitution on the hydrogenation behavior, thermodynamics and structural properties of $La_{1.5}Mg_{0.5}Ni_7$, $La_{1.5}Mg_{0.5}Ni_7H_{9.3}$ and $La_{1.5}Mg_{0.5}Ni_7D_x$ (x=8.9 and 9.1 measured *ex situ* and *in situ*, respectively) have been investigated recently [26]. However this data left open questions concerning the deuterium atom distribution and possible D–D (H–H) distances in such compounds. Thus, the main objective of the present study has been to investigate in details the hydrogen sites configurations in hydride(s)/deuteride(s) of $La_{2-x}Mg_xNi_7$ in order to determine how the presence of Mg affects the possible structural changes and influences the hydrogen capacity.

A_2B_7 intermetallic compounds in the La–Ni system are known to crystallize either with rhombohedral Gd_2Co_7-structure type [27–30] (*R*-3*m*, low temperatures, ~300–1249 K) or hexagonal Ce_2Ni_7-structure type [31] ($P6_3/mmc$, high temperatures, ~1249–1287 K). Both phases belong to the family of compounds built up by AB_5 ($CaCu_5$-structure type, Haucke phases) and AB_2 slabs ($MgZn_2$- and $MgCu_2$-structure type, C-14 and C-15 Laves phases

☆ Laboratory of Crystallography at the University of Geneva has been integrated into the Swiss National Network of Competence MANEP in 2010, thus no longer exists as a separate administrative unit.

* Corresponding author at: Institute for Energy Technology, Physics Department, P.O. Box 40, NO-2027 Kjeller, Norway. Fax: +47 638 10 920.
E-mail address: Matylda.Guzik@ife.no (M.N. Guzik).

0022-4596/$ - see front matter © 2011 Elsevier Inc. All rights reserved.
doi:10.1016/j.jssc.2011.11.026

in the hexagonal and rhombohedral crystal system, respectively) alternating along the [0 0 1] direction with a various ratio [32]. The structure of the hexagonal A_2B_7-type compound can be described as a stacking of $n[AB_2]/m[AB_5]$ (with $n=m=2$, where both types of structural slabs are double). The high temperature ternary derivative of $(La,Mg)_2Ni_7$ reveals the same hexagonal symmetry as the Mg free analog within the similar temperature range of ~1243–1273 K [33]. It has been confirmed that Mg substitutes La atoms only in the AB_2 units [17,21,26,34]. La_2Ni_7 expands anisotropically upon hydrogenation, retaining the symmetry of the intermetallic compound [25]. However recently, it has been suggested that $La_2Ni_7H_{7.1}$ has an orthorhombic distorted structure (space group: *Pbcn*) [10]. In $La_2Ni_7D_{6.5}$ the four D sites are occupied exclusively in $LaNi_2$ slabs [25]. One of them, tetrahedral La_2Ni_2, is present in the parent structure of the intermetallic, while the remaining three sites, two types of octahedral La_3Ni_3 and one tetrahedral La_3Ni, are created upon deuteration. Based on neutron and synchrotron powder diffraction data, Denys et al. have shown that deuteration of $La_{1.5}Mg_{0.5}Ni_7$ leads to an isotropic expansion of the unit cell and formation of deuterides with overall compositions $La_{1.5}Mg_{0.5}Ni_7D_{8.9}$ and $La_{1.5}Mg_{0.5}Ni_7D_{9.1}$ (measured *ex situ* and *in situ*, respectively) [26]. The symmetry of the deuterides is unchanged with respect to the intermetallic compound. In contrast to the nearly ordered $La_2Ni_7D_{6.5}$, the publication by Denys et al. on $La_{1.5}Mg_{0.5}Ni_7D_{8.9(9.1)}$ presents 9 deuterium sites populated exclusively in a disordered way over both AB_2 and AB_5 structural units with occupancy $\leq 50\%$ for 8 of them.

2. Experimental

2.1. Syntheses of intermetallics and their hydrides/deuterides

The syntheses of all intermetallic compounds were performed from high purity elements in two steps (La, Mg, Ni—Merck 99.9%). First, the pieces of La and Ni were arc melted according to the desired composition and then the grinded pellets were mixed with proper amount of Mg powder. The mixture was subsequently pressed in a new pellet, wrapped in tantalum foil and sealed under argon atmosphere in a stainless steel tube. The sample was placed in a furnace under protective argon atmosphere, heated up to 1273 K ($\Delta T=473$ K/h) and kept at this temperature for 10 h. Finally, it was annealed at 1223 K for 4 days and subsequently quenched. In this paper results obtained for two batches of powder with the nominal composition $La_{1.548}Mg_{0.516}Ni_{6.536}$ are presented (see Fig. 1). Their refined compositions differ slightly, thus in the further part of the text a following distinction is introduced: IC_A for $La_{1.64}Mg_{0.36}Ni_7$ and IC_B for $La_{1.63}Mg_{0.37}Ni_7$.

The hydrogenation and deuteration processes were carried out under various conditions. Both samples were activated under dynamic vacuum at ~353 K. 1 g of IC_A powder was then exposed to 10 bar of hydrogen gas at 373 K and left under same conditions for 3 days. As a result, a well crystalline, single phase sample of hydride was obtained. With the same conditions, using deuterium gas instead of hydrogen, a partial sample amorphisation and decomposition of the intermetallic compound took place. To partly eliminate those undesirable effects and knowing that deuteration/hydrogenation properties depend not only on obvious parameters as pressure and temperature but also on less obvious factors as a total sample mass, grain size or deuetration/hydrogenation speed, a mixture of deuterium and argon gas (ratio 1:4) was used. This gave two phases in the deuterated sample of IC_A: D-poor and D-rich phase named alpha- and beta-phase, respectively (see Fig. 2). However, a substantial diffraction peaks broadening was still present in a corresponding powder diffraction pattern. This suggested that rapid deuteration of a fine powder having a significantly large mass could increase a concentration of defects in the structure of both D-poor and D-rich phase. A modulated background was also observed what indicated the presence of an amorphous phase coexisting with crystalline ones. Such a feature in the powder diffraction pattern could also suggest a partial disorder present in the crystalline phases. Thus, one continued with the optimization of synthesis conditions. Further development of synthesis pathway resulted in a single phase sample of the deuteride prepared from IC_B. The deuteration was carried out at room temperature and 5 bar of pure deuterium gas (see Fig. 3) and resulted in a much better sample crystallinity. The collected NPD data showed a significantly lower contribution of the amorphous background and narrower diffraction peaks. The presented beta-phase of IC_B was prepared during an *in situ* powder neutron diffraction experiment.

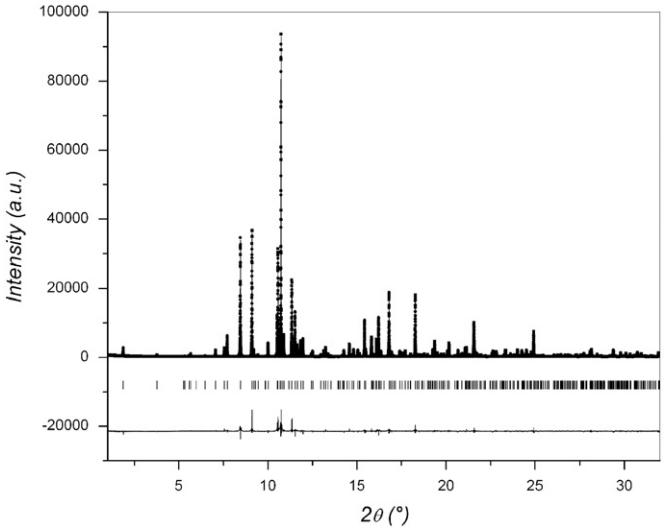

Fig. 1. Observed (points), calculated (line) and difference (bottom line) high resolution SR-PXD patterns ($\lambda=0.40082$ Å) obtained for $La_{1.64}Mg_{0.36}Ni_7$ (IC_A). Vertical bars indicate the positions of Bragg peaks. $\chi^2=4.7$.

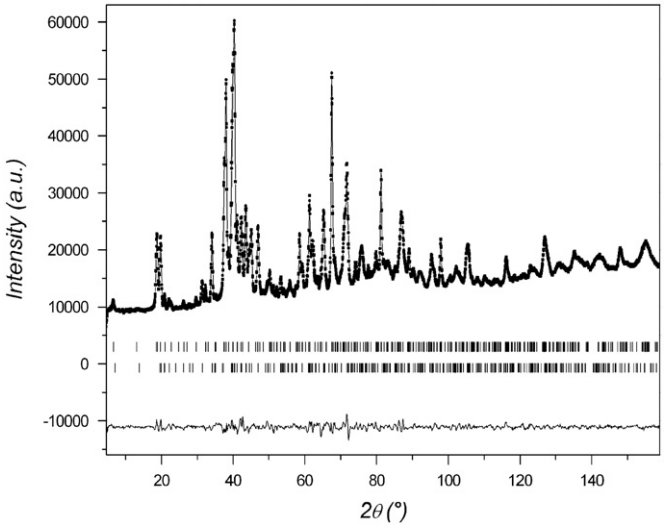

Fig. 2. Observed (points), calculated (line) and difference (bottom line) PND patterns ($\lambda=1.494$ Å) obtained for deuterated sample of IC_A under gaseous mixture of Ar (8 bar) and D_2 (2 bar). Vertical bars indicate the Bragg peaks positions of contributing phases (top: D-rich beta-phase, bottom: D-poor alpha-phase). $\chi^2=8.1$.

2.2. Powder X-ray diffraction (PXD)

Laboratory PXD measurements of intermetallics and hydrides/deuterides were performed with Bruker D8 Advanced diffractometer. High resolution synchrotron radiation powder X-ray diffraction (SR-PXD) experiments were performed at the Swiss-Norwegian beam line (SNBL) at ESRF (Grenoble, France), at the BM01B station (λ=0.40082 and 0.52002 Å). Some of the samples were measured at the BM01A station (λ=0.72756 Å) with MAR345 image plate at different sample-to-detector distances. In all SR-PXD experiment the powders were sealed in boron-glass capillaries (d=0.2 mm) (see Fig. 1).

2.3. Powder neutron diffraction (PND)

Ex situ and *in situ* PND measurements were carried out with the HRPT diffractometer (λ=1.494 Å) at SINQ (Villigen, Switzerland). For the *ex situ* experiment the sample was loaded into a vanadium container and sealed with indium wire to avoid any desorption of deuterium. During the *in situ* measurements, the powder was introduced into an airtight stainless steel container (see Figs. 2 and 3).

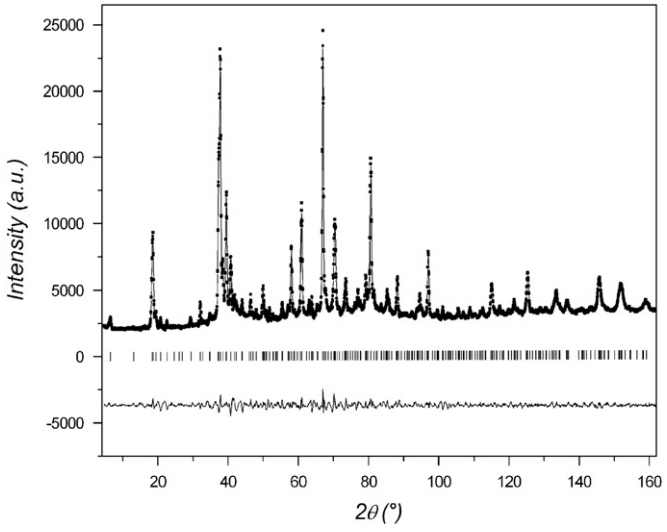

Fig. 3. Observed (points), calculated (line) and difference (bottom line) PND patterns (λ=1.494 Å) obtained during ex situ measurements of $La_{1.63}Mg_{0.37}Ni_7D_{8.8}$.Vertical bars indicate the Bragg peaks positions. χ^2=7.4.

2.4. Pressure–composition isotherm (PCI) measurement

Thermal stability and hydrogen storage capacity of the IC_B deuteride were studied with the Sieverts apparatus PCTPro-2000 from HyEnery. 0.6176 g of powder was evacuated under dynamic vacuum at room temperature for 5 h and subsequently at 573 K overnight. PCI data were collected during absorption under up to 6.4 bar deuterium pressure at 308 K for a total measuring time of 750 h and desorption down to 10^{-5} bar deuterium pressure during 255 h at the same temperature.

2.5. Structure refinements

In order to determine the distribution of deuterium atoms the parallel tempering algorithm in the *FOX* program [35,36] was used. All Rietveld refinements were performed with *FULLPROF* [37]. X-ray scattering factors and neutron cross-sections were taken from the *FULLPROF* library. The laboratory PXD and SR-PXD refinement backgrounds were modeled by interpolations between manually chosen points. Due to a presence of the modulated background, especially pronounced in the PND pattern of the deuterated two-phase sample, 12-coefficient Fourier-cosine polynomial and Fourier filtering procedure were used to fit the PND data. This method allowed to refine global temperature displacement parameter for D-poor and D-rich phase and eliminated the negative values of some thermal parameters during refinement of beta-phase of IC_B (see Table 3). Pseudo-Voigt and Thompson–Cox–Hasting pseudo-Voigt profile function were applied to model peaks shape.

3. Results and discussion

3.1. Metal atom substructure

3.1.1. Intermetallic compounds

SR-PXD data (see Fig. 1 and Table 1) confirmed the high purity of the samples, even though the final refined compositions differed from the nominal $La_{1.548}Mg_{0.516}Ni_{6.536}$. The well crystalline phase reveals close similarity to La_2Ni_7 but with reduced unit cell parameters due to the smaller magnesium radii (see Table 2). This suggests the substitution by Mg in the structure even though a significant loss of Mg was observed during sample preparation, 1.35 and 1.48 wt% of Mg for IC_A and IC_B, respectively, after annealing treatment vs. 2.05 wt% of Mg in samples before the reaction. Based on the SR-PXD data, the crystal structure of

Table 1
Rietveld refinement results on SR-PXD data for two batches of $La_{2-x}Mg_xNi_7$ (nominal composition: $La_{0.774}Mg_{0.258}Ni_{3.268}$).

Refined composition		$La_{1.64}Mg_{0.36}Ni_7$ (IC_A)					$La_{1.63}Mg_{0.37}Ni_7$ (IC_B)				
Instrument Wavelength		High resolution diffractometer (SNBL) 0.40082 Å					High resolution diffractometer (SNBL) 0.52002				
Space group		$P6_3/mmc$					$P6_3/mmc$				
Cell parameters		a=5.04914(1) Å					a=5.04731(8) Å				
		c=24.3229(1) Å					c=24.3186(4) Å				
		V=537.009(3) Å^3					V=536.52(2) Å^3				
Crystal structure*											
Atom	**Wyckoff position**	***x***	***y***	***z***	B_{iso}	**Occup**	***x***	***y***	***z***	B_{iso}	**Occup.**
La 1	***4f***	1/3	2/3	0.02771(6)	0.91(4)	0.64(1)	1/3	2/3	0.02698(8)	1.03(6)	0.63(1)
La 2	***4f***	1/3	2/3	0.17086(5)	0.85(3)	1.01(1)	1/3	2/3	0.17108(6)	0.98(4)	1.00(1)
Mg 1	***4f***	1/3	2/3	0.02771(6)	0.91(-)	0.36(-)	1/3	2/3	0.02698(8)	1.03(-)	0.37(-)
Ni 1	***2a***	0	0	0	0.84(8)	1.00(-)*	0	0	0	0.9(1)	1.00(-)*
Ni 2	***4e***	0	0	0.1684(1)	0.94(5)	1.00(-)	0	0	0.1678(1)	0.98(7)	1.00(-)
Ni 3	***4f***	1/3	2/3	0.83306(9)	0.55(4)	1.00(-)	1/3	2/3	0.8329(1)	0.61(6)	1.00(-)
Ni 4	***6h***	0.8327(6)	0.665(1)	1/4	0.37(4)	1.00(-)	0.8326(8)	0.665(2)	1/4	0.50(6)	1.00(-)
Ni 5	***12k***	0.8331(4)	0.6661(8)	0.08485(5)	0.54(3)	1.00(-)	0.8330(5)	0.666(1)	0.08486(6)	0.84(4)	1.00(-)

* During preliminary refinements Ni atoms occupancies did not vary more than ±5%, thus during final refinement all of them were fixed to 100%.

Table 2
Comparison of selected crystallographic parameters for chosen hexagonal A_2B_7-type compounds and their deuterides in La–Ni and La–Mg–Ni systems.

Parameters	Compound						
	La_2Ni_7 [51]	$La_2Ni_7D_{6.5}$ [25]	$La_{1.5}Mg_{0.5}Ni_7$ [26]	$La_{1.5}Mg_{0.5}Ni_7D_{8.9}$ [26]	$La_{1.63}Mg_{0.37}Ni_7$ (IC_B)	$La_{1.64}Mg_{0.36}Ni_7D_{0.56}$ (alpha-phase of IC_A)	$La_{1.63}Mg_{0.37}Ni_7D_{8.8}$ (beta-phase of IC_B)
a [Å]	5.058	4.9534	5.0285	5.3854	5.0473	5.1041	5.4151
c [Å]	24.71	29.579	24.222	26.437	24.3186	24.8824	26.5392
V [Å^3]	547.47	628.52	530.42	664.01	536.52	561.39	673.95
V_{AB5} [Å^3]	177.37	171.96	175.77	216.47	177.20	183.42	217.73
V_{AB2} [Å^3]	96.35	142.30	89.01	115.24	91.05	97.28	119.25
$\Delta a/a$ [%]	–	−2.1	−0.6	7.1	−0.2	1.1	7.3
$\Delta c/c$ [%]	–	19.7	−2.0	9.1	−1.6	2.3	9.1
$\Delta V/V$ [%]	–	14.8	−3.1	25.2	−2.0	4.6	25.6
$\Delta V_{2xAB5}/V_{2xAB5}$ [%]	–	−3.1	−0.7	24.6	−0.1	3.5	22.9
$\Delta V_{2xAB2}/V_{2xAB2}$ [%]	–	47.7	−7.6	29.8	−5.5	6.9	31.0

Table 3
Rietveld refinement results on neutron data for beta-phase of $La_{2-x}Mg_xNi_7$–D system.

Refined composition	$La_{1.64}Mg_{0.36}Ni_7D_{7.19(5)}$ (deuteride of IC_A—multiphase sample)				$La_{1.63}Mg_{0.37}Ni_7D_{8.8(1)}$ (deuteride of IC_B—single phase sample)				
Instrument	*HRPT* at SINQ (Villigen)				*HRPT* at SINQ (Villigen)				
Wavelength	1.494 Å				1.494 Å				
Space group	$P6_3/mmc$				$P6_3/mmc$				
Cell parameters	a=5.3854(3) Å				a=5.4151(1) Å				
	c=26.336(2) Å				c=26.539(1) Å				
	V=661.50(6) Å^3				V=673.95(4) Å^3				
Fraction	49.6(9) wt%				100 wt%				
Crystal structure									
Atom	**Wyckoff position**	***x***	***y***	***z***	**Occup.**	***x***	***y***	***z***	B_{iso}	**Occup.**
La 1	**4*f***	1/3	2/3	0.0085(6)	0.64(-)	1/3	2/3	0.0135(6)	3.7(3)	0.63(-)
La 2	**4*f***	1/3	2/3	0.1753(5)	1.00(-)	1/3	2/3	0.1758(4)	1.1(1)	1.00(-)
Mg 1	**4*f***	1/3	2/3	0.0085(6)	0.36(-)	1/3	2/3	0.0135(6)	3.7(-)	0.37(-)
Ni 1	**2*a***	0	0	0	1.00(-)	0	0	0	0.9(1)	1.00(-)
Ni 2	**4*e***	0	0	0.1719(5)	1.00(-)	0	0	0.1702(3)	1.3(1)	1.00(-)
Ni 3	**4*f***	1/3	2/3	0.8348(4)	1.00(-)	1/3	2/3	0.8323(3)	2.2(1)	1.00(-)
Ni 4	**6*h***	0.829(3)	0.658(5)	1/4	1.00(-)	0.839(2)	0.678(4)	1/4	1.36(9)	1.00(-)
Ni 5	**12*k***	0.840(2)	0.681(3)	0.0876(2)	1.00(-)	0.835(1)	0.670(2)	0.0885(2)	2.37(8)	1.00(-)
D 1	**6*h***	0.495(2)	0.505(2)	1/4	0.75(3)	0.503(1)	0.497(1)	1/4	3.2(1)	1.00(-)
D 2	**4*e***	0	0	0.1039(9)	0.65(3)	0	0	0.1062(6)	3.2(-)	1.00(-)
D 3	**12*k***	0.354(7)	0.177(4)	0.1520(4)	0.64(2)	0.349(8)	0.175(4)	0.1512(4)	3.2(-)	0.67(2)
D 4	**12*k***	0.480(3)	0.520(3)	0.0570(8)	0.52(2)	0.485(1)	0.515(1)	0.0712(7)	3.2(-)	0.66(2)
D 5	**12*k***	0.336(4)	0.168(2)	0.0355(5)	0.64(2)	0.325(6)	0.163(3)	0.0231(4)	3.2(-)	0.77(2)
		$B_{iso\_overall}$=2.30(4) Å^2								

$(La,Mg)_2Ni_7$ seems to retain the hexagonal Ce_2Ni_7-structure type (see Table 1). The unit cell parameters for samples IC_A and IC_B do not differ significantly suggesting that the syntheses give repeatable results. The Rietveld refinements show that Mg partly substitutes La, exclusively in the $LaNi_2$ slabs (4*f* site) and occupies statistically ~37% of the available sites. Compared to pure La_2Ni_7, the contraction of the unit cell due to the introduced Mg for IC_B is: $\Delta V/V=-2.0\%$ with $\Delta a/a=-0.2\%$ and $\Delta c/c=-1.6\%$, without any change of the symmetry (hexagonal, $P6_3/mmc$). The volume of double layer of the AB_2 units in IC_B, with the refined composition corresponding to $La_{1.26}Mg_{0.74}Ni_4$, significantly contracts, $\Delta V_{AB2}=-5.5\%$, because of the large difference in the atomic radii of La (1.877 Å) and Mg (1.602 Å). Selective occupation of Mg in the La sites shortens the La–La interatomic distances in the AB_2 slabs as compared to the Mg free analog with (La,Mg)–(La,Mg) 3.196 Å and La–La 3.394 Å, respectively. Due to contraction in the basal *ab* plane of the unit cell, minor changes also proceed in the AB_5 layers, $\Delta V_{AB5}=-0.1\%$. Results for IC_A are listed in Table 2. These data are in agreement with published ones [17,21,26,34].

3.1.2. Hydride/deuterides

Upon hydrogenation/deuteration $La_{2-x}Mg_xNi_7$ behaves differently from A_2B_7-type compounds, e.g. La_2Ni_7–D [25] or Ce_2Ni_7–D [23,24,38]. Both La_2Ni_7 and Ce_2Ni_7 expand significantly, $\Delta V/V=14.9\%$ and 21.1%, but only in one direction with $\Delta c/c=19.9\%$ and 21.5%, respectively, and thus represent so called anisotropic hydrides. $La_{1.63}Mg_{0.37}Ni_7D_{8.8}$ (beta-phase of IC_B) also reveals a significant expansion, $\Delta V/V=25.6\%$, but the volume increases isotropically and almost equally in the [0 0 1] direction and in the basal *ab* plane, $\Delta a/a=7.3\%$ and $\Delta c/c=9.1\%$, respectively (see Tables 2 and 3). Upon hydrogenation/deuteration, the occupancy of the 4*f* site by the Mg atoms remains unchanged (see Table 3). However, the presence of Mg influences drastically the distribution of deuterium atoms in the structure. For the La_2Ni_7 and Ce_2Ni_7 deuterides [23,25,38], deuterium atoms are situated exclusively within the AB_2 units, while in $La_{1.63}Mg_{0.37}Ni_7D_{8.8}$ both the AB_2 and AB_5 structural slabs host D atoms (see Fig. 4). Mg substitution increases the hydrogen storage capacity by making the AB_5 units deuterium-active with a resulting isotropic expansion of the lattice.

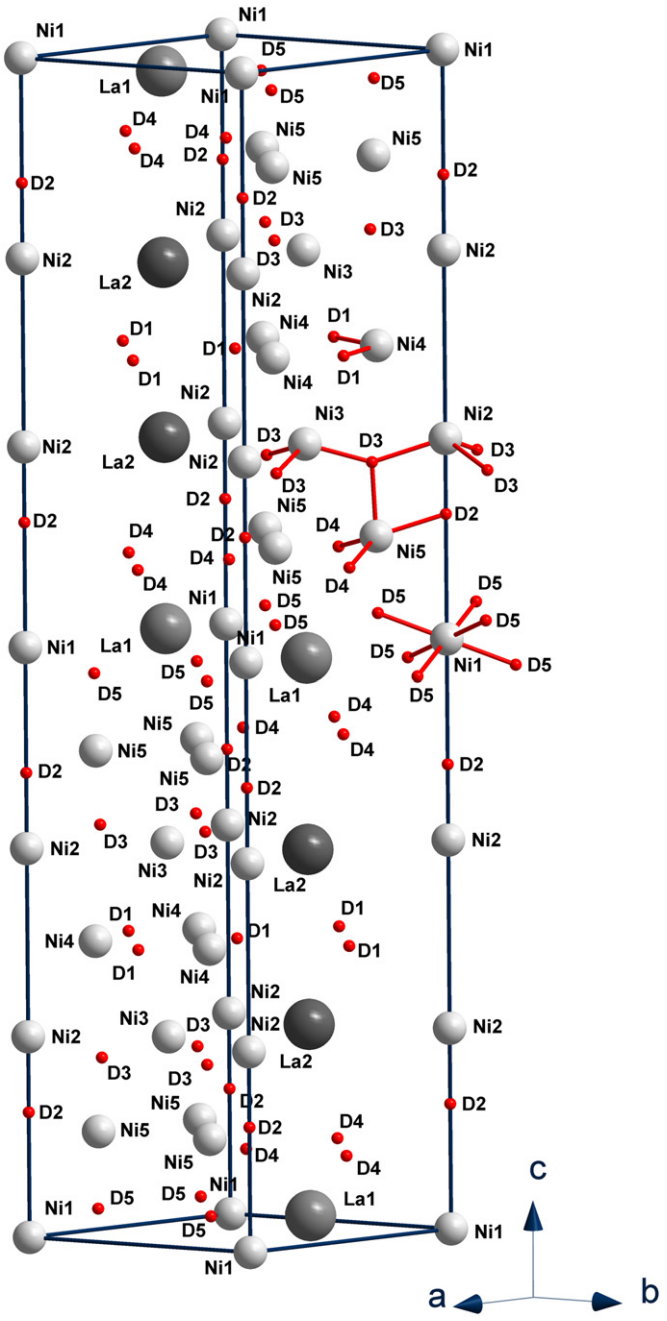

Fig. 4. Crystal structure of the beta-phase of $La_{2-x}Mg_xNi_7$ ($La_{1.63}Mg_{0.37}Ni_7D_{8.8}$ and $La_{1.64}Mg_{0.36}Ni_7D_{7.19}$). For atoms labeling see Table 3.

The lattice of the second, hitherto unknown alpha-phase with the refined composition $La_{1.64}Mg_{0.36}Ni_7D_{0.56}$ expands also almost isotropically upon deuteration, but the effect is rather weakly pronounced ($\Delta V/V=4.6\%$, $\Delta a/a=1.1\%$, $\Delta c/c=2.3\%$, see Table 2 and Table 4). The symmetry of this phase is the same as for the intermetallic compound.

3.2. Deuterium site configurations

The distribution of deuterium atoms in $La_{1.63}Mg_{0.37}Ni_7D_{8.8}$ is comparable with the previously reported $La_{1.5}Mg_{0.5}Ni_7D_{8.9(9.1)}$, but the occupied positions differ significantly. This could be related to the contribution of Mg atoms to the structure. For the present $La_{1.63}Mg_{0.37}Ni_7D_{8.8}$, a satisfactory fit between the calculated and observed powder diffraction data is obtained with D atoms in only five sites (see Figs. 1, 3, 4 and Table 3), and thus opposite to the reported nine sites for $La_{1.5}Mg_{0.5}Ni_7D_{8.9(9.1)}$ [26]. D1 and D3–D5 are present in the model by Denys et al., while the D2 is located in the same type of site (4*e*) but with different value of *z*-coordinate compared to [26]. The remaining four deuterium atom positions reported for $La_{1.5}Mg_{0.5}Ni_7D_{8.9(9.1)}$ have not been found in the present work. A summary of the distribution of the D atoms is given as follows (see Fig. 4):

- D1 is located within the La_2Ni_2 tetrahedron in the AB_5 structural unit. The site exists in the parent structure of the intermetallic compound. It is equivalent to D2 in $La_{1.5}Mg_{0.5}Ni_7D_{8.9(9.1)}$ and has no analog in $La_2Ni_7D_{6.5}$ [25];
- D2 is located close to the boundary between the AB_5 and AB_2 slabs, and within the Ni_4 tetrahedron. The same type of site (4*e*) is occupied in $La_{1.5}Mg_{0.5}Ni_7D_{8.9(9.1)}$ (D3) but the *z*-coordinate differs, 0.1062(6) vs. 0.2176(6), respectively. The site is equivalent to D1 in $La_2Ni_7D_{6.5}$;
- D3 is located in the La_2Ni_4 deformed octahedron within the AB_5 slabs. This interstice is equivalent to D4 in $La_{1.5}Mg_{0.5}Ni_7D_{8.9(9.1)}$ and has no analog in the Mg-free deuteride;
- D4 is located in the $(La,Mg)_2Ni_2$ tetrahedron in the AB_2 units and close to the boundary between the slabs. It is equivalent to D6 in $La_{1.5}Mg_{0.5}Ni_7D_{8.9(9.1)}$ and is comparable to D4 in $La_2Ni_7D_{6.5}$;
- D5 is located in the AB_2 slabs, within the trigonal bipyramid $(La,Mg)_3Ni_2$. It is an analog of D7 in the $La_{1.5}Mg_{0.5}Ni_7D_{8.9(9.1)}$ and D3 in the $La_2Ni_7D_{6.5}$.

No additional sites were determined in $La_{1.63}Mg_{0.37}Ni_7D_{8.8}$. $La_{1.5}Mg_{0.5}Ni_7D_{8.9(9.1)}$ and $La_{1.63}Mg_{0.37}Ni_7D_{8.8}$ differ significantly in a view of the D sites occupancies (see Table 3). In $La_{1.63}Mg_{0.37}Ni_7D_{8.8}$ the D1 and D2 positions are fully occupied while in $La_{1.5}Mg_{0.5}Ni_7D_{8.9(9.1)}$ the occupancies of the similar sites are equal to 77% and 50% (fixed), respectively. The occupancies of D3, D4 and D5 in $La_{1.63}Mg_{0.37}Ni_7D_{8.8}$ are partial and between 66% and 77%, while for $La_{1.5}Mg_{0.5}Ni_7D_{8.9(9.1)}$ the occupancies of equivalent sites are 46%, 40% and 50%, respectively. The hydrogenation/deuteration leads to expansion of both types of slabs, 22.9% for AB_5 and 31.0% for AB_2 in the most saturated beta-phase (see Table 2) with deuterium atoms occupying both types of structural blocks almost evenly. The refined compositions of slabs account for $AB_5D_{4.5}$ and $AB_2D_{4.3}$, in the $La_{1.63}Mg_{0.37}Ni_7D_{8.8}$. The deuterium sublattice in the AB_5 slabs is essentially the same as reported for $LaNi_5D_7$ [39] and includes three D positions: La_2Ni_2 (D1/occupancy=1.00), Ni_4 (D2/occupancy=1.00) and La_2Ni_4 (D3/occupancy=0.67). For latter one, the D3 atom is shifted from the center of La_2Ni_4 by ~0.02 Å towards Ni5 and thus reveals a rather uncommon triangular metal coordination (Ni2, Ni3 and Ni5) with Ni–D distances: 1.71(4), 1.55(4) and 1.67(1) Å, respectively. Such surrounding has been observed for the $LaMgNi_4$–H system [2] and some saline metal hydrides (*T*Mg_2H_7, *T*—La, Ce, Sm) [40,41]. The lattice parameters of the double AB_5 unit in $La_{1.63}Mg_{0.37}Ni_7D_{8.8}$ ($a=5.415$ Å and $c=8.574$ Å) are similar to $LaNi_5D_6$ [42] ($a=5.410$ Å and $c=8.586$ Å, double cell in *z* direction). Opposite to $La_{1.5}Mg_{0.5}Ni_7D_{8.9(9.1)}$, partial ordering of deuterium atoms on the 4*e* and 6*h* sites is observed within this type of slabs. The total hydrogen uptake in AB_5 layers is smaller in present $La_{1.63}Mg_{0.37}Ni_7D_{8.8}$ than in previously investigated $La_{1.5}Mg_{0.5}Ni_7D_{8.9(9.1)}$. In these subunits, volume increase of the all occupied polyhedra is observed compared to the H(D)-free intermetallic. The estimated volume changes correspond to 17%, 16% and 19% for D1 (La_2Ni_2), D2 (Ni_4) and D3 (La_2Ni_4), respectively.

Two deuterium sites have been determined within the AB_2 layers: D4 in $(La,Mg)_2Ni_2$ and D5 in $(La,Mg)_2Ni_2$ with occupancy 66% and 77%, respectively. The structure of these units resembles

Table 4
Rietveld refinement results on PND data for alpha-phase of $La_{1.64}Mg_{0.36}Ni_7$–D system.

Refined composition		$La_{1.64}Mg_{0.36}Ni_7D_{0.56(2)}$ (deuteride of IC_A—multiphase sample)				
Instrument		*HRPT* at SINQ (Villigen)				
Wavelength		1.494 Å				
Space group		$P6_3/mmc$				
Cell parameters		$a=5.1041(3)$ Å				
		$c=24.882(2)$ Å				
		$V=561.39(7)$ Å^3				
Fraction		50.5(8) wt%				
Crystal structure						
Atom	**Wyckoff position**	***x***	***y***	***z***	B_{iso}	**Occup.**
La 1	***4f***	1/3	2/3	0.0263(3)	0.6(2)	0.64(-)
La 2	***4f***	1/3	2/3	0.1719(6)	1.1(1)	1.00(-)
Mg 1	***4f***	1/3	2/3	0.0263(3)	0.6(-)	0.36(-)
Ni 1	***2a***	0	0	0	0.6(2)	1.00(-)
Ni 2	***4e***	0	0	0.1744(3)	0.8(1)	1.00(-)
Ni 3	***4f***	1/3	2/3	0.8310(4)	1.5(1)	1.00(-)
Ni 4	***6h***	0.840(2)	0.679(4)	1/4	0.8(1)	1.00(-)
Ni 5	***12k***	0.837(1)	0.674(2)	0.0866(1)	1.00(7)	1.00(-)
D 1	***4f***	2/3	1/3	0.0597(5)	0.1(3)	0.56(2)

closely hydrides/deuterides of $MgZn_2$-type compounds [43] with four RE_2Ni_2 interstitial sites available for deuterium atoms. In the present study only two of them are populated. This is different from what has been reported for the same slabs in $La_{1.5}Mg_{0.5}Ni_7D_{8.9(9.1)}$ and most of the C-14 Laves phase deuterides where deuterium atoms occupy at least three or all tetrahedral RE_2Ni_2-type sites in a disordered way. Furthermore, in $La_{1.63}Mg_{0.37}Ni_7D_{8.8}$ none of the $RENi_3$ sites is filled with D atoms. Even though the distances between deuterium sites in the AB_2 slabs for $La_{1.63}Mg_{0.37}Ni_7D_{8.8}$ exceed 1.9 Å, no ordering of deuterium sublattice is found. Similar to $La_{1.5}Mg_{0.5}Ni_7D_{8.9(9.1)}$, D5 is shifted into the common triangular face of the $(La,Mg)_2Ni_2$ tetrahedron and thus coordinated by a trigonal bipyramid $(Mg/La)_3Ni_2$. The refined composition of the AB_2 layers accounts for $La_{0.63}Mg_{0.37}Ni_2D_{4.3}$. Deuterium content is higher than in the $LaMgNi_2D_{3.8}$ layer for $La_{1.5}Mg_{0.5}Ni_7D_{8.9(9.1)}$ but lower than in the Mg free analog [25]. The estimated volume change of the occupied interstices equals 30% and 18% for D4 ($(La,Mg)_2Ni_2$) and D5 ($(La,Mg)_3Ni_2$), respectively. The higher change obtained for $(La,Mg)_2Ni_2$ tetrahedron could explain the much higher volume expansion observed for the AB_2 slabs compared to AB_5 ones. A possible reason is a presence of Mg that reveals high hydrogen affinity and thus results in a higher occupancy of such sites in general. Interatomic distances for atoms coordinating interstitial sites in $La_{1.63}Mg_{0.37}Ni_7D_{8.8}$ and $La_{1.5}Mg_{0.5}Ni_7D_{8.9(9.1)}$ are comparable suggesting similar expansion of corresponding polyhedra in both compounds upon deuteration. Observed variations in the deuterium atoms distribution in $La_{1.63}Mg_{0.37}Ni_7D_{8.8}$ and $La_{1.5}Mg_{0.5}Ni_7D_{8.9(9.1)}$ give different arrangements of deuterium around the nickel atoms. For $La_{1.63}Mg_{0.37}Ni_7D_{8.8}$ all five Ni atoms located in both types of slabs have deuterium atoms as their nearest neighbors. The surrounding is similar to what was previously observed in $ErNi_3D_x$ [44], $HoNi_3D_4$ [45], $Ce_2Ni_7D_{\sim 4}$ [24,38], where the Ni atoms reveal a tendency to be surrounded by D atoms in tetrahedral or tetrahedral-like configurations as in some complex transition metal hydrides [46–48]. In our cases, the same feature is apparent (see Fig. 4). Only one of five Ni atoms (Ni5) is surrounded by deuterium in a deformed tetrahedral configuration and displaying Ni–D bond lengths and D–Ni–D angles in the range of 1.62–1.71 Å and 76–120°, respectively. For Ni2, Ni3 and Ni4 such tendency can be clearly seen as rigid, trigonal pyramids and thus similar to the structure of $ErNi_3D_{1.3}$ [44]. The Ni–D bond lengths and D–Ni–D bond angles vary in the range of 1.55–1.71 Å and 112–115°, respectively. The deuterium atoms around Ni1 form a disordered and deformed saddle-like configuration. The average distance from Ni to the surrounding D5 is equal to 1.65 Å and the angles vary from 73° to 180°. The shortest observed D–D distance is equal to 1.96(3) Å (D5–D5). Selected interatomic distances are listed in Table 5.

3.2.1. Hydrogen/deuterium induced site depopulation

In the alpha-phase only one site (4*f*) within the AB_2 slabs is partially occupied (see Table 4). This site is located in the $LaNi_3$ tetrahedron and is no longer populated in the beta-phase. This phenomenon showing depopulation of hydrogen sites as a function of hydrogen concentration is relatively rare in transition metal based metal hydrides. However, there exist few examples of such behavior in the literature, e.g. depopulation of Ni_4 and $LaNi_3$ sites in the $LaMgNi_4$–H system, Ho_6 site in the Ho_6Fe_{23}–H system, La_4Pd_2 interstitial site in La_3Pd_5Si–H system, $ErCo_3$ interstice in $ErCo_3$–H system and $(Ti,Zr)_4$ type sites in the $Ti_{0.64}Zr_{0.36}Ni$–H system [2]. Some of these structural features could be rationalized by atomic size considerations and repulsive H–H interactions originating from the proximity of the other occupied interstices. However, some cases clearly suggest the presence of other structure determining factors, for example directional metal–hydrogen bonding [46], metal–hydrogen bond strength [49], and distribution of paired electron density [50]. In the present alpha-phase the size of the occupied site is relatively big with $r=0.45$ Å and thus it could easily accommodate deuterium/hydrogen atoms. On the other hand, the size of the same hole in the D-rich beta-phase is even bigger ($r=0.49$ Å), but it remains unfilled. Such behavior could indicate that repulsive D–D interactions are likely to influence the non-occupancy of certain interstices. The 4*f* site in the beta-phase, is presumably unoccupied because of its proximity to occupied $(La,Mg)_2Ni_2$ tetrahedron (D–D ~ 1.45 Å).

3.3. Pressure–composition relationship

The PC isotherm (see Fig. 5) exhibits a sloped equilibrium plateau pressure attributed to coexistence of the alpha- and beta-phase. The maximum hydrogen capacity at 308 K is high, D/f.u. = 10.18, thus comparable with values obtained for the Mg free analog at 263 K with H/f.u. = 10 [26], and higher than for $La_{1.5}Mg_{0.5}Ni_7$ with H/f.u. = 9 at 298 K [26]. The deuterium storage capacity obtained during the PCI experiment is higher than values

Table 5
Selected interatomic distances (Å) in $La_{1.63}Mg_{0.37}Ni_7D_{8.8}$ from PND data (cut-off values: 3.0 Å and 1.8 Å for D and Ni atoms' environments, respectively).

D atoms' environment				Ni atoms' environment	
D1–La2	2.53(1) × 2	D4–(La1,Mg1)	2.09(2) × 2	Ni1–D1	1.64(3) × 4
D1–Ni4 × 2	1.58(1) × 2	D4 – (La1,Mg1)	2.82(2) × 2	Ni1–D1	1.64(4) × 4
D1–D1	2.66(1) × 2	D4 – La2	3.12(2)	Ni2–D2	1.70(2)
D1–D1	2.75(1) × 2	D4 – Ni5	1.71(1)	Ni2–D3	1.71(4) × 2
D2–Ni1	2.18(12)	D4 – Ni5	1.71(1)	Ni2–D3	1.71(5) × 2
D2–Ni2	1.70(2)	D4 – D2	2.866(9) × 2	Ni3–D3	1.55(4) × 2
D2–Ni5	1.620(8) × 2	D4 – D3	2.66(3) × 2	Ni3–D3	1.55(5) × 2
D2–Ni5	1.62(1)	D4–D4	2.46(1)	Ni4–D1	1.58(1)
D2–D3	2.03(3) × 2	D4–D4	2.95(1)	Ni4–D3	1.58(2)
D2–D3	2.03(5) × 2	D4–D5	2.09(3) × 2	Ni5–D2	1.620(8)
D2–D4	2.866(9) × 2	D4–D5	2.93(2) × 4	Ni5–D3	1.67(1)
D2–D4	2.87(1) × 4	D5–(La1,Mg1)	1.87(3)	Ni5–D4	1.71(1) × 2
D2–D5	2.68(2) × 2	D5–(La1,Mg1)	2.72(4) × 2	Ni5–D4	1.74(1)
D2–D5	2.866(3) × 2	D5–Ni1	1.64(3)		
D3–Ni2	1.71(4)	D5–Ni5	1.74(1)		
D3–Ni3	1.55(4)	D5–D2	2.68(2)		
D3–Ni4	2.625(1)	D5–D4	2.09(3) × 2		
D3–Ni5	1.666(1)	D5–D4	2.93(2) × 2		
D3–D2	2.03(3)	D5–D4	2.93(3) × 2		
D3–D3	2.58(4)	D5–D5	1.96(3)		
D3–D3	2.58(7) × 2	D5–D5	1.96(4) × 2		
D3–La2	2.79(5)	D5–D5	2.64(3)		
D3–La2	2.78(5)	D5–D5	2.65(5) × 2		
D3–D3	2.83(4)	D5–D5	2.78(3)		
D3–D3	2.83(7) × 2	D5–D5	2.78(5) × 2		
D3–D4	2.66(4) × 2				

refined from PND data but still lower than one could expect for a deuteride with a full occupancy of all determined D sites (what would account for $La_{1.63}Mg_{0.37}Ni_7D_{11.5}$). The equilibrium plateau pressure in deuterium absorption and desorption at 308 K is observed at ~0.58 bar and ~0.07 bar, respectively. For the studied compound only one hydrogen charging cycle was performed. However, it is known that absorption isotherms tend to change during first cycles in these types of compounds. Thus, in order to compare a hydride stability with similar intermetallic compounds, only desorption isotherms have been taken into account. Interestingly, the different Mg contribution affects the stability of $La_{2-x}Mg_xNi_7$ hydrides. Based on the obtained data, it seems that $La_{1.63}Mg_{0.37}Ni_7D_x$ forms more stable deuteride/hydride than $La_{1.5}Mg_{0.5}Ni_7H_x$ with 0.15 bar desorption equilibrium pressure at 298 K [26]. The present value is also significantly lower than in $La_2Ni_7H_x$ with 0.6 bar at 273 K [10] and $La_{1.4}Mg_{0.6}Ni_{5.6}Co_{1.0}H_x$; 0.3–0.5 bar at 333 K [11]. $Ce_2Ni_7H_x$ with 0.065 bar desorption equilibrium pressure at 313 K [23], has almost the same deuteride/hydride stability as $La_{1.63}Mg_{0.37}Ni_7D_x$.

A subsequent decrease in deuterium pressure to ambient conditions during 255 h at 308 K caused the sample to desorb deuterium only partially with release of 8.35 D/f.u.

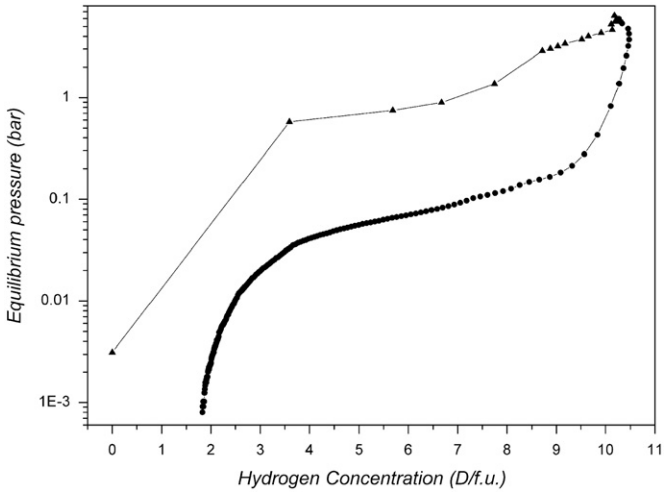

Fig. 5. Pressure-composition isotherm of $La_{1.63}Mg_{0.37}Ni_7$–D system during absorption (upper line, triangles) and desorption (lower line, circles) at 308 K.

4. Conclusions

The present study confirms an important influence of Mg atoms on the distribution of hydrogen/deuterium in hydrides/deuterides of $La_{2-x}Mg_xNi_7$. Observed Mg substitution within the AB_5 slabs results in occupation of only 5 interstitial sites in the D-rich beta-phase and one interstitial site in the D-poor alpha-phase. The latter is different from any occupied site in the saturated hydride/deuteride. Obtained results suggest that both H–H (D–D) repulsive interactions and tendency to create directional transition metal–hydrogen bonding are the main factors responsible for the arrangement of D atoms in the investigated crystal structures of $La_{1.63}Mg_{0.37}Ni_7D_{8.8}$ and $La_{1.63}Mg_{0.37}Ni_7D_{0.56}$.

Acknowledgment

The authors thank Prof. Y. Filinchuk (Institute of Condensed Matter and Nanosciences, Université Catolique de Louvain, Belgium) who dedicated his beam time at BM01A station (SNBL, Grenoble) to collect some of the data. This work was supported by the HyTRAIN program of the Marie Curie Research Training Network funded under the EC's 6th Framework Human Resources and Mobility Program.

Appendix A. Supplementary information

Supplementary data associated with this article can be found in the online version at doi:10.1016/j.jssc.2011.11.026.

References

[1] E. Akiba, H. Hayakawa, T. Kohno, J. Alloys Compd. 408-412 (2006) 280–283.
[2] J.N. Chotard, D. Sheptyakov, K. Yvon, Z. Kristallogr. 223 (2008) 690–696.
[3] H. Hayakawa, H. Enoki, E. Akiba, J. Jpn. I Met. 70 (2006) 158–161.
[4] K. Kadir, T. Sakai, I. Uehara, J. Alloys Compd. 257 (1997) 115–121.
[5] K. Kadir, T. Sakai, I. Uehara, J. Alloys Compd. 302 (2000) 112–117.
[6] T. Kohno, H. Yoshida, F. Kawashima, T. Inaba, I. Sakai, M. Yamamoto, M. Kanda, J. Alloys Compd. 311 (2000) 5–7.
[7] G. Renaudin, L. Guenee, K. Yvon, J. Alloys Compd. 350 (2003) 145–150.
[8] T.Z. Si, Q.A. Zhang, N. Liu, Int. J. Hydrogen Energy 33 (2008) 1729–1734.
[9] F.L. Zhang, Y.C. Luo, J.P. Chen, R.X. Yan, J.H. Chen, J. Alloys Compd. 430 (2007) 302–307.
[10] K. Iwase, K. Sakaki, Y. Nakamura, E. Akiba, Inorg. Chem. 49 (2010) 8763–8768.
[11] Y. Chai, K. Asano, K. Sakaki, H. Enoki, E. Akiba, J. Alloys Compd. 485 (2009) 174–180.
[12] Y.J. Chai, K. Sakaki, K. Asano, H. Enoki, E. Akiba, T. Kohno, Scr. Mater. 57 (2007) 545–548.
[13] A. Ferey, F. Cuevas, M. Latroche, B. Knosp, P. Bernard, Electrochim. Acta 54 (2009) 1710–1714.
[14] H. Hayakawa, E. Akiba, M. Gotoh, T. Kohno, Mater. Trans. 46 (2005) 1393–1401.
[15] J. Nakamura, K. Iwase, H. Hayakawa, Y. Nakamura, E. Akiba, J. Phys. Chem. C 113 (2009) 5853–5859.
[16] Y. Nakamura, J. Nakamura, K. Iwase, E. Akiba, Nucl. Instrum. Meth. A 600 (2009) 297–300.
[17] T. Ozaki, M. Kanemoto, T. Kakeya, Y. Kitano, M. Kuzuhara, M. Watada, S. Tanase, T. Sakai, J. Alloys Compd. 446 (2007) 620–624.
[18] D.H. Wang, Y.C. Luo, R.X. Yan, F.L. Zhang, L. Kang, J. Alloys Compd. 413 (2006) 193–197.
[19] F.L. Zhang, Y.C. Luo, J.P. Chen, R.X. Yan, L. Kang, J.H. Chen, J. Power Sources 150 (2005) 247–254.
[20] F.L. Zhang, Y.C. Luo, K. Sun, D.H. Wang, R.X. Yan, L. Kang, J.H. Chen, J. Alloys Compd. 424 (2006) 218–224.
[21] F.L. Zhang, Y.C. Luo, D.H. Wang, R.X. Yan, L. Kang, J.H. Chen, J. Alloys Compd. 439 (2007) 181–188.
[22] J. Zhang, F. Fang, S.Y. Zheng, J. Zhu, G.R. Chen, D.L. Sun, M. Latroche, A. Percheron-Guegan, J. Power Sources 172 (2007) 446–450.
[23] R.V. Denys, V.A. Yartys, M. Sato, A.B. Riabov, R.G. Delaplane, J. Solid State Chem. 180 (2007) 2566–2576.
[24] Y.E. Filinchuk, K. Yvon, H. Emerich, Inorg. Chem. 46 (2007) 2914–2920.
[25] V.A. Yartys, A.B. Riabov, R.V. Denys, M. Sato, R.G. Delaplane, J. Alloys Compd. 408 (2006) 273–279.
[26] R.V. Denys, A.B. Riabov, V.A. Yartys, M. Sato, R.G. Delaplane, J. Solid State Chem. 181 (2008) 812–821.
[27] J. Dischinger, H.J. Schaller, J. Alloys Compd. 312 (2000) 201–210.
[28] L.B. Liu, Z.P. Jin, Z. Metallkd. 91 (2000) 739–743.
[29] T. Yamamoto, H. Inui, M. Yamaguchi, K. Sato, S. Fujitani, I. Yonezu, K. Nishio, Acta Mater. 45 (1997) 5213–5221.
[30] L.G. Zhang, H.Q. Dong, J.F. Nie, F.G. Meng, S. Jin, L.B. Liu, Z.P. Jin, J. Alloys Compd. 491 (2010) 123–130.
[31] N.S. Bilonizh, Russ. Metall. (1972) 130–133.
[32] E. Parthe, R. Lemaire, Acta Crystallogr. B 31 (1975) 1879–1889.
[33] S. Negri, M. Giovannini, A. Saccone, J. Alloys Compd. 439 (2007) 109–113.
[34] R.V. Denys, B. Riabov, V.A. Yartys, R.G. Delaplane, M. Sato, J. Alloys Compd. 446 (2007) 166–172.
[35] R. Cerny, Z. Kristallogr. 223 (2008) 607–616.
[36] R. Cerny, V. Favre-Nicolin, Z. Kristallogr. 222 (2007) 105–113.
[37] J. Rodriguez-Carvajal, Physica B 192 (1993) 55–69.
[38] Y.E. Filinchuk, K. Yvon, J. Alloys Compd. 446 (2007) 3–5.
[39] P. Thompson, J.J. Reilly, L.M. Corliss, J.M. Hastings, R. Hempelmann, J. Phys. F 16 (1986) 675–685.
[40] F. Gingl, K. Yvon, T. Vogt, A. Hewat, J. Alloys Compd. 253 (1997) 313–317.
[41] H. Kohlmann, F. Werner, K. Yvon, G. Hilscher, M. Reissner, G.J. Cuello, Chem.—Eur. J 13 (2007) 4178–4186.
[42] P. Fischer, A. Furrer, G. Busch, L. Schlapbach, Helv. Phys. Acta 50 (1977) 421–430.
[43] V.A. Yartys, V.V. Burnasheva, K.N. Semenenko, N.V. Fadeeva, S.P. Solovev, Int. J. Hydrogen Energy 7 (1982) 957–965.
[44] Y.E. Filinchuk, K. Yvon, J. Alloys Compd. 404 (2005) 89–94.
[45] Y.E. Filinchuk, D. Sheptyakov, K. Yvon, J. Alloys Compd. 413 (2006) 106–113.
[46] K. Yvon, in: A. Zuttel, A. Borgschulte, L. Schlapbach (Eds.), Hydrogen as a Future Energy Carrier, Wiley-VCH, Weinheim, 2008, pp. 195–208.
[47] K. Yvon, in: K.H.J. Buschow (Ed.), Encyclopedia of Materials: Science and Technology, Elsevier, Oxford, 2004, pp. 1–9.
[48] K. Yvon, G. Renaudin, in: R.B. King (Ed.), Encyclopedia of Inorganic Chemistry, John Wiley & Sons Ltd., New York, 2005, pp. 1814–1846.
[49] I. Jacob, J.M. Bloch, D. Shaltiel, D. Davidov, Solid State Commun. 35 (1980) 155–158.
[50] P. Vajeeston, P. Ravindran, R. Vidya, A. Kjekshus, H. Fjellvag, Europhys. Lett. 72 (2005) 569–575.
[51] K.H.J. Buschow, A.S. Van Der Goot, J. Less-Comm. Mat. 22 (1970) 419–428.